ON THE ARCING PHENOMENA IN THE MHD CHANNEL*

V. Goldfarb, C. Pian, I. Sadovnik
Avco Research Laboratory, Inc.
Everett, MA 02149

ABSTRACT

Experimental and analytical studies have been carried out to characterize and further understand arcing phenomena with particular emphasis on erosion produced by arcs populating high-voltage (open) interelectrode gaps.

This paper presents a set of related studies, each address a specific aspect of the arcing phenomena. First, bench top experiments were conducted to examine arcing behavior in a magnetic field as the arcs moved among bare and slagged electrodes. Direct observation of arcing in an MHD generator was then made on the Mark VII channel sidewall, and these results were correlated with measured voltage distributions.

Arcing erosion was measured in both the bench top and generator experiments for various electrode configurations. Erosion of copper electrodes was compared to erosion rates calculated from a thermal ablation model for stationary and/or moving arcs.

Finally, a discussion is presented on some specific features of the arc behavior and on consequences of cathodic arcing.

INTRODUCTION

The lifetime of an MHD channel is limited by the gradual deterioration and/or catastrophic damage due to arcing, primarily on the cathode wall. Cathode wall non-uniformities can lead to axial breakdowns both over the high-voltage intercathode gaps and across the sidewall insulator gaps. The erosion induced by these arcs can be reduced or tolerated in a number of ways:

- Decrease the Hall field strength
- Generate more uniform axial voltage distributions
- Lower the current density or increase arc root mobility over electrode surfaces
- Select materials able to withstand high arc thermal fluxes and/or electrochemical erosion
- Use "sacrificial" or renewable electrodes

Some of these methods will degrade generator performance or will necessitate impractical designs. Others have not yet been tried.

This paper, while not attempting to solve the arcing problem, provides additional insight into the multi-faceted arcing phenomena. Experimental observations and measurements as well as analytical studies will consider the following subjects:

- Anode and cathode arcing features in laboratory bench tests
- Voltage distributions and arc characteristics in an MHD generator
- Electrode erosion by stationary and moving arcs predicted by an analytical model

BENCH ARCING EXPERIMENTS

Bench-scale experiments were conducted to simulate and observe the salient features of interelectrode arcing even though some features, such as adequate combustion gas flow over the surface and a moving slag layer, proved difficult to duplicate. These experiments first investigated arc damage to interanode insulators, then studied arcing behavior on the cathode wall both with and without slag.

Arcing and Damage to Interanode Insulators

Interanode breakdown and subsequent arcing is severely damaging because the J x B forces drive the arcs into the wall and the supporting backwall. The electrical properties of such arcs are described in Refs. (1) and (2), while experimental observations of interanode arcing in a generator were made in Ref. (3). Refs. (4) and (5) confirm that interanode insulator damage may be reduced by changing anode geometry.

This experimental study focused on characterizing interanode arcing in a magnetic field and reducing the possibility of damage by arc quenching. The test rig shown in Figure 1 was used, where the insulators consisted of BN or Si_3N_4, 25 mm x 15 mm in cross-section and 1-10 mm thick, clamped between water-cooled copper electrodes. The arc current was provided by a 300 V, 40 A rectifier, and a water-cooled Helmholtz pair provided magnetic field strengths up to 1.45 T. After the arc was initiated with a high frequency starter, interelectrode arc currents and voltages were recorded (Figure 2). The insulators were weighed upon completion of the test to measure the mass of evaporated material. For this series of tests, the burn time was 4-8 sec, the arc voltage was 80-120 V, and the mass loss was 40-400 mg. Data from a typical test series is shown in Table 1. From these experiments, the following observations were made:

- Energy expenditure for BN arc "cutting" is about 1 J/mg, independent of the magnetic field strength. For a gap current above some minimum value I_{cr}, which is a function of magnetic field strength, this energy increases with current.
- The cutting rate of BN is about 5 mm/sec and decreases slightly as specific arc power (power/gap thickness) increases.
- As the insulator thickness increases the specific power remains constant while the specific energy for ablation decreases, indicating that arc power is more efficiently utilized.
- Hot pressed silicon nitride plates were more easily cut by arcing than the boron nitride ones. Since both specific energy

and specific power were lower for Si_3N_4, the thermal (arc) ablation rate for these materials does not correlate to erosion/corrosion resistance or hardness, in which Si_3N_4 is superior to BN.

To prevent propagation of an arc that has been driven into an insulator by the magnetic force, the arc must be extinguished somewhere along its trajectory. One possible technique may be adapted from magnetic blast switch technology: quenching an arc by blowing it into a chamber where interelectrode spacing abruptly increases.

Experiments were performed using BN spacers, with an 8 mm wide cavity formed by machining the sides of two adjacent electrodes. Arcs were observed to initiate normally, but then disappear after reaching the edges of the cavity and cutting through the top of the insulator (Figure 3). The width itself of the cavity could not account for the arc quenching since the open circuit voltage was high enough to sustain the arc. Instead, it is concluded that the sudden increase in width extinguished the arc. It is then important to determine whether repeated arcing would eventually cut through the remaining insulation to strike the back board. Such a break through did occur, but only after repeated arc initiations (7-15) at the same location with high voltages and currents. MkVII channel tests support the possibility of limiting the depth of arc propagation: only about 1 cm arc propagation was observed after 15 minutes when subjected to an externally applied 10-20 A interanode arc in a 2 T magnetic field.

Slagged Intercathode Arcing

The first series of intercathode bench top experiments studied arc breakdown in the presence of a molten slag layer. A seed/ash mixture was transported by argon through a gas-cooled enclosure over electrodes separated by a BN spacer. A magnetic field of up to 1 T was directed parallel to the length of the interelectrode gap.

Figure 4 shows the time-resolved discharge current and voltage for various modes of operation. In the absence of a magnetic field, the 8-12 A arc burns quietly inside the "cavity" formed in the molten slag. The arc voltage is low due to metal vapor in the cavity. Diffuse current transfer could also occur in this mode, given the proper slag thickness and temperature. At higher currents the slag evaporates and the arc burns openly, surrounded by a slag pool, at a low and stable voltage.

The magnetic field was observed to exert a moderate influence on the current through the slag. At increasing field strengths, the voltage increased as the current channel was deflected to the top of the slag layer, elongating the current path. The influence of the magnetic field on an open arc, though, is quite strong. At higher magnetic fields with the same current, the voltage increases several times and periodic fluctuations of both current and voltage appear. The frequency ranges of these fluctuations fell around 1 and around 100 Hz. Molten slag frequently forms "bridges" which reduce the voltage and also suppress the current fluctuations.

The arc originates as a breakdown through the slag-filled gap, then expands radially toward the walls of the enclosure. Slag and a jet of plasma erupt noisily from the opening in the enclosure. The erratic nature of the arcing prevented any determination of current or magnetic field dependence. However, the heat flux to the electrodes increases greatly in the presence of a magnetic field, with about 70 percent of the total electrical energy transferred to the electrodes. The anode side of the intercathode arc receives a larger fraction of the total heat.

Anodic erosion rates are significantly higher (Table 2) so that damage is concentrated on the anode edge. Platinum and tungsten-copper caps eroded somewhat less than the copper ones. The arc remains stationary for tens of seconds before changing positions. Therefore the electrode surfaces and anode edges wear rather uniformly, and only averaged and smoothened arc traces could be observed in post-test study. For example, traces on the platinum surface are 200-400 mm wide and 10-20 mm deep.

Unslagged Intercathode Arcing

During the second series of experiments, arcs were monitored between open unslagged electrodes in the device pictured in Figure 5. Water-cooled copper electrodes could be positioned at various angles with respect to the imposed magnetic field, and they were adjusted so that the Lorenz force drew the arc away from the surface. The channel environment was simulated by spreading a cesium seeded flame from an oxy-acetylene burner over the electrodes. Electrical and heat flux measurements were taken along with optical spectra of the discharge. Arc development and movement were recorded with a movie camera.

In the first group of tests, the electrodes were oriented parallel to the magnetic field. Figure 6 shows the development of individual arcs: the arc first spreads radially from the edges of the gap and forms a semicircle in a well-defined vertical plane. The arc roots slide over the electrodes. Next, several concentric current channels may appear, each with its own electrode spots. In the final phase these channels disappear sequentially, leaving a short-lived luminous cloud. This behavior did not vary substantially over the test ranges of 0.02-0.10 T and 10-30 A.

The movie camera was too slow (500 frames/sec, 10^{-4} sec exposures) to capture all the details of the process, but instantaneous features can be observed from the frame sequences. Normally the current goes to zero and the voltage goes to its open circuit level when the new arc does not start before the original one extinguishes. In some cases, though, an arc will elongate to reach a high voltage, allowing a new arc to form while the original one still burns. These simultaneous arcs lead to higher I_{min} and lower V_{max}. The lifetime of an individual arc is 5-10 msec, and the velocity of the arc column and arc spots is about 5 m/sec. Particulates from the erosion process sometimes emerge from the gaps at a velocity of 20-70 m/sec. The presence of hot combustion gases only decreases the amplitude of current pulsations due to an increase in I_{min} and some increase in final arc length. This relative insensitivity to the combustion gases is to be expected because the

arc properties are defined by the metal vapor jets that emerge from the arc spots. These jets have a much higher conductivity than even seeded combustion products.

The erosion rate was comparable to the values for slagged electrodes. Again, this is to be expected since the erosion is primarily dependent on current and heat transfer in the arc rather than on the atmosphere and surface chemistry. The atmosphere and chemistry, though, could influence the motion and residence time of the arc spots. As before, the anode erosion was higher than that of the cathode despite the symmetrical arc propagation.

Gradual changes in electrode orientation alter the arc behavior. Arc movement along the gap predominates, while regular radial expansion subsides. Current and voltage pulsations become erratic and have smaller amplitudes than before. Movie frames shown in Figure 7 where the magnetic field is perpendicular to the top of the electrode (simulating a sidewall) reveal only one or two arcs existing simultaneously. Starting near the middle of the gap, the arc elongates irregularly and moves in the direction of the Lorentz force. The arc roots may move partly along the edges (especially of the anode) and partly across the top surface at about 2-6 m/sec. The arc appears to be anchored by the anode spot position, with the cathode spot moving freely. It is unclear whether the arc spot motion is continuous or jumping. After the arc channel moves to its next position, luminous clouds produced either by plasma afterflow or continuing diffuse current remain visible for about 1 msec.*

The gas flow around the arc gap was visualized by adding sodium and strong turbulence was observed. The arc generated turbulent convection only moderately increases the heat flux to the electrodes despite a significant increase in the arc voltage. Most of the energy is dissipated to the surrounding atmosphere where it is moved away from the electrodes by "arc blow".

Erosion rates with the arc moving along the interelectrode gap are the lowest compared to an arc burning in the absence of a magnetic field. To supplement weight loss measurements, erosion rate comparisons were made by measuring the intensities of the copper emission lines. The CuI lines radiated by the stationary arc are an order of magnitude stronger than those radiated by moving arcs at the same current. Higher anode erosion rates could result from either higher heat fluxes or lower mobility of the anode spots. Arc spot mobility is a function of the surface conditions. In these experiments the surface of the copper anodes was oxidized while the cathode surface appeared to be cleaned by sputtering. The low conductance oxide film on the anode can restrict mobility and increase the residence time of the anode spots by delaying the start of anode spot motion after breakdown. Alternatively, the gas flow field could blow the arc spot away from the cathode edge to reduce the erosion rate there.

* The role of the glow discharge/residual current in the arc reignition was studied quite recently in Ref. 10.

Comparing the bench test results with the MHD channel erosion data shows similar (0.5-1.0 μg/C) erosion rates, supporting the conclusion that rapid movement of the interelectrode arcs produces comparatively little erosion of the cathode and sidewall elements. The arcs are driven by Lorentz forces. On the sidewall these forces result from the main component of the magnetic field; at the cathode a small (0.01-0.10 T) magnetic field exists perpendicular to the wall, either as a component of the main field lines if the wall is tilted by as little as 1μ or as a spacial inhomogenity in the magnetic field.

MK VII SIDEWALL VOLTAGE DISTRIBUTION AND ARCING OBSERVATIONS

Sidewall Voltage Distribution

Forty pegs on the left sidewall of the Mk VII channel were instrumented with voltage transducers to resolve the axial (V_x) and transverse voltage distributions (V_y). It was observed that

- V_y "overshoots" are larger at the colder wall, especially for copper anodes, with both slagged and unslagged walls
- Large non-uniformities in V_x on the unslagged cathode wall "propagate" across the sidewall in decreasing magnitude until, at the mid-height of the channel, the axial voltages are nearly uniform. With a slag layer the same features are observed but they exhibit larger scatter. Close to the anode wall the axial voltage distribution becomes even more uniform.

A two-dimensional voltage distribution reconstructed from the axial traverses is shown in Figure 8. Vertical voltage differences (DV_y) are usually smaller than the corresponding axial voltage differences (DV_x). The largest voltage difference, though, exists in the diagonal direction perpendicular to equipotentials, and may be even higher than the cathode voltage differences. These voltage jumps produce the peg erosion seen on the edges of the first two peg rows.

Formation of voltage distributions may be conveniently studied on both the cathode and anode walls by reversing the direction of the magnetic field. Voltage distribution near the "new" anode is very non-uniform immediately after the field reversal.

Voltage distributions were also measured in the central region of the bar sidewall. In these experiments the interbar voltages could be increased or lowered from their nominal values by connecting the appropriate bars to anodes or cathodes.

Correlating the erosion pattern and the voltage non-uniformity at the sidewall could predict erosion of differently designed sidewalls without long-duration testing. Since the cathode non-uniformities only propagate a few rows along the sidewall, the sidewall lifetime could be lengthened by replacing these rows with non-conducting ceramic elements.

Sidewall Arcing

A special viewing port (Figure 9) was installed in the right sidewall to permit observation of arcing on the opposite wall. A 2-in.-diameter, 2-ft-long electrically insulated tube passes through the magnet bore. The diameter of the tube limits the field of view to 4-6 sidewall bars or pegs. The tube is gas purged, and gas pressure pulses remove the slag and dust that collect in it.

Interpeg Arcing and Sidewall Arc Radiation

With no B-field, interpeg arcing induced by an external power supply was observed for both clean and slagged sidewalls. In seeded flow and unslagged walls, a single 5-20 A arc burns rather steadily at 50-80 V. The arc is swept along by the flow (Figure 10a), elongating until it breaks off and starts again at point A. With slag, the arc impedes the flow so that the slag separates around it and leaves a clean surface downstream (Figure 10b). About 60 percent of the arc thermal energy or 100 to 200 W goes to the electrode, which is sufficient to evaporate approximately 0.5 g/sec of molten slag. At a typical slag flow velocity of 2 cm/sec, this rate of evaporation will clear a 2 mm x 5 mm strip.

Optical spectra of sidewall arc radiation were taken (Figure 11) which revealed that, in addition to radiation from the hot gas flow, strong lines of copper (CuI) and calcium (CaI and CaII) are present. The copper originates from peg erosion while the calcium appears from the slag vapors. The intensity ratios of the copper lines (Cu I 5105, Cu I 5153, and Cu I 5218) were used to derive the arc column temperature. Using known transition probabilities, the temperature was calculated as T = 6030 ± 200 K. This temperature was comparable to that of an air-burning arc. In addition, comparison of the radiation from an arc sustained by an external source and from a high cathode open gap arc in a magnetic field could be used to evaluate the Hall arc current, which is normally difficult to measure directly.

Interbar Arcing

Interbar voltages were measured and the arcing pattern was simultaneously photographed with a 200-mm lens for the bars seen through the optical window (31M, 31B, 32M, and 32B). Optical spectra were also taken with a fiberoptics-connected spectrometer. No arcing was observed under normal operation when DV, measured between 31M and 32B, was lower than 50 V. When DV was increased above 50 to 65 V by applying an external dc voltage or by connecting bars to cathodes, arcing took place if the seeded gas conductivity exceeded 3 mho/m. Three to six arcs with currents of 2-3 A each usually occurred on unslagged bars. Sometimes these arcs suddenly merged into one large arc with a power supply limited current of 10-20 A. When DV crossed the threshold voltage in slagged flow, a more stable 5-10 A arc formed. In some cases, though, a current up to 10 A could flow without forming an observable arc. It is possible that an arc was indeed present but was running within the slag layer.

Motion pictures taken under the conditions indicated in Figures 17 and 18 prompted the following observations and measurements:

- Under normal operation, the maximum "diagonal" voltage ($30\ V < \Delta V_d < 50\ V$) is a factor of 1.2 to 1.5 times DV_x but is not high enough for arc formation. Increasing DV_d to 60-70 V with an external power supply, or by connecting to certain electrodes can induce arcing, presumably by increasing the total or local Hall voltage.

- Above the voltage threshold, strong arc "pulses" form every 0.05-0.25 second on unslagged surfaces, lasting for 0.1-0.2 second. The current in these interbar arcs start as 0.5-2 A in the discharge and then increases to over 10 A for the strong arc in 0.05-0.01 second.

- Several small arc spots or 1 to 2 large spots exist permanently and move slowly (a few cm/sec) over the liquid slag surface. The spot polarity is difficult to identify, as is the position of the "opposite" arc root. It is not clear if these arcs originate from the neighboring wall element or if they run between the slag surface and the core plasma, where diffuse current transfer takes place. It is impossible to distinguish the "Faraday" and "Hall" arcs.

- More distinct arcs were observed when the magnetic field was reversed. These arcs are localized and move rapidly between the bars along the same diagonal where the highest voltage occurs.

- Bar edge erosion was evident in post-test inspection. It is believed that only arcs with roots directly attached to the metal, especially short "surface-to-surface" interelement arcs, cause significant damage while arcs rooted on the slag surface do not cause erosion.

ANALYTICAL ESTIMATE OF ARCING EROSION

In this section we calculate the erosion of electrode material due to the heat load imposed at the foot of either a moving or stationary arc. The heat load can be calculated from the electrical power dissipated at the arc root. This power is equal to the near electrode arc voltage drop times the arc current. For the case of the intercathode high gap arc, the voltage drop is related to the local gap properties. Local gap properties are associated with the physical state of the gap and include insulator width, slag thickness, slag chemistry, and wall temperature, among others. On the other hand, the currents flowing across the intercathode high gap arcs are strong functions of the overall generator operating parameters, such as channel loading, average plasma conductivity, and magnetic field strength. The voltage is believed not to scale with generator size, while the intercathode gap current will increase with generator size.

The anodic and cathodic drops of the intercathode high gap are assumed in the present analysis to be approximately 1/3 of the total high gap voltage (the other 1/3 consumed in the arc

column). So that for a 75V gap each drop amounts to 25V. We have also estimated the cathode wall axial current leakage to be about 20A for the AVCO MkVI generator. So we can use 500W as a typical number for the heat load of these intercathode high gap arc roots. The arc is assumed to be described by a 2-dimensional gaussian distribution of heat flux q (W/m^2) with a total arc heat load Q (W) using the following equations:

GEOMETRY FOR ARC HEAT LOAD MODEL

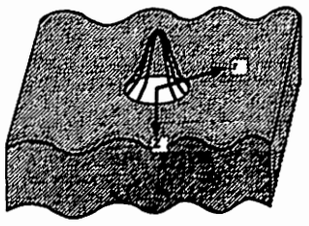

$$q = q_{max} e^{-k_c r^2} \quad (1)$$

$$Q = \frac{\pi q_{max}}{k_c} \quad (2)$$

where q_{max} is the maximum heat flux at the arc center and $R_{arc} = k_c^{-1/2}$ is the characteristic arc radius. Assuming that the heat load of this arc is imposed on a semi-infinite electrode, approximating that the depth of the electrode in the Z direction is much larger than R_{arc}, the time dependent temperature distribution may be found.[11,12] If the arc is moving over the electrode surface at velocity V, the temperature at the center of the moving arc (r=0) as a function of time and depth coordinate (Z_m) in the moving frame of reference can be expressed as:

$$T(Z_m,t) = \frac{2Q}{(4\pi)^{3/2} k \sqrt{a}} \int_0^t \frac{e^{-\frac{Z_m^2}{4at'} - \frac{V^2}{4a}\left(\frac{1}{4ak_c} + t'\right)}}{\sqrt{t'}\left(\frac{1}{4ak_c} + t'\right)} dt' \quad (3)$$

denoting the thermal conductivity and diffusivity of the electrode material as k and a, respectively. The erosion rate of a moving arc G (kg/sec) can then be stated as the simple relation:

$$G = \rho_{elec} \, V \frac{Z_{evap}}{\sqrt{k_c}} \quad (4)$$

where ρ_{elec} is the electrode material density and Z_{evap} is the depth in the electrode at which the temperature reaches the evaporation temperature of the electrode material. This erosion rate equation can be substituted into the temperature equation at $T=T_{evap}$. However, for quasi-steady operation ($t \to \infty$) it is also necessary to subtract the power required to melt (ΔH_{melt}) and vaporize (ΔH_{evap}) electrode material due to the arc heat load Q. Therefore the following integral equation is derived which can be used to find the erosion rate G as a function of the electrode properties, arc velocity, arc radius, and arc heat load:

$$T_{evap} = \frac{2(Q - (\Delta H_{melt} + \Delta H_{evap})\, G)}{(4\pi)^{3/2} k \sqrt{a}} \cdot \int_0^\infty \frac{e^{-\frac{G^2 k_c}{4at' V^2 \rho^2_{elec}} - \frac{V^2}{4a}\left(\frac{1}{4ak_c} + t'\right)}}{\sqrt{t'}\left(\frac{1}{4ak_c} + t'\right)} dt' \quad (5)$$

Note that the unknown G appears both inside and outside the integral. This solution, though, breaks down at small velocities where the erosion rate, defined in Eq. 4, approaches zero. Since actual erosion rates for stationary arcs are much larger than those for large arcs, an alternate solution must be obtained for the motionless arc. Therefore the stationary arc erosion rate is defined as:

$$G_s = \frac{\rho_{elec}}{k_c} \frac{dZ_{evap}}{dt} \quad (6)$$

The erosion rate now depends on the time derivative of the evaporation depth Z_{evap} evaluated at time t_{evap}, which is the time needed for the electrode surface under the stationary arc to reach the evaporation point. Inserting this new equation into the previous temperature equation with V=0, results in the following integro-differential equation for the stationary arc:

$$T_{evap} = \frac{2(Q - (\Delta H_{melt} + \Delta H_{evap})\, \rho_{elec} \frac{dZ_{evap}}{dt}}{(4\pi)^{3/2} k \sqrt{a}} \cdot \frac{}{k_c} \int_0^t \frac{e^{-\frac{Z_{evap}^2 k_c}{4at'}}}{\sqrt{t'}\left(\frac{1}{4ak_c} + t'\right)} dt' \quad (7)$$

The evaporation time is simple to obtain in closed form by setting $Z_{evap}=dZ_{evap}/dt=0$ and integrating the previous equation. Both equations were also solved numerically over a range of arc radii for a copper electrode and an arc heat load of 500 W. A "blended" solution for $G(V,R_{arc})$ has been constructed using the stationary erosion rate at small velocities and the moving arc solution for medium to large arc velocities. The results are shown in Figure 14 for an arc radius of 0.2 mm. From the solution it was found that there exists for every arc radius a critical arc velocity, denoted as V*, above which no erosion occurs. For the 0.2 mm arc investigated, this critical velocity is 0.8 m/sec.

A characteristic erosion rate has been defined as the erosion rate for an arc velocity that is half of the critical velocity; that is, G*=G(V*/2). For the test case shown in Figure 14, G*=2.5 mg/sec. The functional dependence of G(V) can be investigated for all R_{arc} once the arc velocity is nondimensionalized by V* and the erosion rate is nondimensionalized by G*. The curves of $V^*(R_{arc})$ and $G^*(R_{arc})$ in Figure 15 show that both critical velocity and characteristic erosion decrease with

arc radius. In addition, a critical arc radius, R_{arc}^*, exists beyond which no erosion occurs, even for a stationary arc. This critical radius is calculated as .25 mm for 500 W arcs on copper electrodes.

A simplified set of equations are presented to simulate the erosion rate for 500 W copper arcs as a function of the radius:

$$\frac{G}{G^*} = 1.2\left(1 - \frac{V}{V^*}\right)^{1/4} \quad ; \quad G^* = 25\left(1 - \frac{R_{arc}}{R_{arc}^*}\right); \tag{8}$$

$$V^* = 16\left(1 - \sqrt{\frac{R_{arc}}{R_{arc}^*}}\right)$$

where G* is in mg/sec and V* is in m/sec. A 3-dimensional plot of G as a function of arc velocity and arc radius to critical radius ratio, constructed from the simplified equations, is shown in Figure 16. A similar 3-D description of arcing erosion might be developed by consolidating the effect of electrode material and arc heat load into the critical arc radius.

Figure 16 shows the region for the arc radius very cose to the critical radius. This was done since typical characteristic erosion rates for 20A arcs from the model's results are around 500 μg/coulomb (at $R_{arc}/R_{arc}^* \sim 0.5$). Measured levels for arcing erosion in bench experiments yield much smaller numbers ~ 2 μg/coul. This rate can be attained by either of 2 situations: a) motionless arcs with radius very close to the critical radius, which is the case described in Fig. 21, b) arcs of arbitrary radius (smaller than R_{arc}^*) which move at velocities very close to the arc critical velocity. Of course the second criterion can be explained by arcs which are most of the time mobile with arbitrarily large velocities (larger than V^*), but for a small fraction of their time are stationary, and erode the electrode at this small time fraction. In this case it would mean that typically arcs are stationary less than 1 percent of the time.

DISCUSSION OF CATHODIC ARCING FEATURES

Although arcing takes place on both the cathode and anode walls, erosion of the anode wall is less severe since the lower interelectrode voltage "spikes" infrequently produce arcing. Even if arcing does occur, proper design of the inter-electrode space can limit the damage. Therefore it is more crucial to develop a broad understanding of "cathodic" arcing, including near-cathode sidewall elements where the voltage distribution and arcing breakdown conditions are similar to those of the cathode. This similarity arises from both the sidewall/cathode electrical link and the formation of a potassium sub-layer over the sidewall following this link. Although propagation of the sidewall arc in the boundary layer and the velocity of the arc root may be different from those at the cathode, sidewall erosion is probably not qualitatively different from cathode erosion. The ability of the "finer" sidewall segmentation to split leakage current into multiple smaller arcs may be offset by these smaller elements being more susceptible to damage.

Figure 17 illustrates the formation of characteristic "cathode" voltage patterns and arcing for a 10 electrode wall segment. The voltage over the segment depends on the overall channel conditions, so it was necessary to assume some typical voltages: 80 V arcing breakdown voltage, 70 V steady-state arc voltage, and 1 V voltage drop across a shorted gap. The latter voltage was selected for illustrative purposes since the actual voltage drop is quite small. The voltage distribution and arcing sequence is thus:

1. Initially the slag layer has uniform resistance so that the gap voltages are all equal.
2. The voltage is redistributed by the random formation of the potassium-rich slag layer, which changes selective gap resistances.
3. As this redistribution continues, most gap resistances decrease with the available voltage "concentrating" over the few "unshorted" gaps.
4. As gap #2 gradually shorts, the voltage at gap #7 reaches breakdown level.
5. An arc forms at gap #7 and runs along the gap length, carrying 70 V and a current which, is a function of the overall channel conditions. The arc removes the potassium sub-layer (one traverse of a 100 to 500 W arc is sufficient), but liquid slag continues to flow over the gap, except near the arc where arc jetting blows the slag away. The liquid slag across the gap has a relatively high resistance and therefore does not short the gap.
6. The arc extinguishes but the gap still remains highly resistive. It is unclear whether the gap voltage then remains the same or decreases.
7. Gap #2 and gap #7 are now both highly resistant but "arc-less" and the first one to reach breakdown voltage, in this case gap #2, arcs. Thus the voltage in gap #7 drops.
8. Gap #2 arcs for a period of time.
9. The arc across gap #2 disappears so that gap #2 competes with the gap with the "next highest resistance", in this case gap #9.
10. Gap #2 wins again. After a new breakdown, the arc on gap #2 re-establishes.

Some features of this process merit further comments:

Single vs. Multiple Arcs

The arc mode depends on the shape of the V-I characteristics. In most cases the "minimum voltage" principle is valid for arc discharges and implies that the merger of small arcs should take place when operating on the falling branch of the V-I characteristic and not on the rising branch. The branch on which the arc operates is dependent on the operating conditions as follows:

Falling Branch	Rising Branch
Free-burning arc	Arc channel diameter limited by walls
High concentration of metal vapors in arc channel	Cold gas flow
Strong conductivity rise with temperature	Small inter-electrode distance
	Weak conductivity rise with temperature

Consequently, arcs with high current (over a few A) that evaporate electrode material, slag, and/or seed deposits belong to the first category and tend to run "solo". In contrast, low current "non-evaporating" arcs whose small diameter is controlled by the "cold"gas flow in the boundary layer belong to the second category and may exist as a several-member "family". These arcs include those between the core plasma flow and the electrode surfaces.

Several strong arcs may coexist, but they must have separate power supplies to keep their roots electrically isolated in order to maintain them simultaneously.

Arc Movement

Arc movement over an electrode surface is a function of the magnetic field (strength and direction), the electrode material properties which control the surface temperature, and the presence of an insulating oxide layer, a conductive seed/-potassium layer, and the slag. To a lesser extent, the arc movement is also dependent on the temperature and electrical conductivity of the gas boundary layer. Arc velocity over very clean copper electrodes has been defined in Ref. 9 as $V = 5\ B^{0.6}\ (I/d)^{0.4}$.

High current "evaporating" arcs tend to stay a site which is hot or is covered with a conductive layer or to move along the gap "in search of" potassium deposits. These arcs tend to evaporate as much low-ionization potential material as possible into their current channels to lower their resistances. Low current arcs do not incorporate electrode material and are therefore less surface dependent and more mobile. Since electromagnetic force is current dependent, the correlation of actual arc velocity versus current may be much more complicated.

Arcing Erosion

Bench tests indicate that the erosion rate for a typical 20 A moving arc is on the order of 2 µg/C, which on the average is 0.05 mg/sec. Assuming that the removal of 10 g copper can be tolerated, the electrode would have a lifetime on the order of 100 hr at this erosion rate. This prediction is somewhat pessimistic compared to better results obtained in long duration channel tests. Actual arcing erosion may also be reduced by several factors:

- The open gap moves along the channel
- The effective duration of the arc is reduced by spending part of the time transferring current in the diffuse mode.
- Some of the calculated leakage current actually flows without damage into the liquid slag and the boundary layer rather than across the electrode gap. A diagram of such behavior, showing the current density in the arcing cross-section of an open gap and in a shorted gap, is shown in Figure 18.

Arc Extinguishing

Bench experiments indicate that an arc is blown into cold surrounding gas, where it disappears, if the available voltage cannot support a certain arc length. Same should be true for the "cathodic" MHD channel arc (except the arc column diffuses reaching the core flow). It can be speculated that high current arcs controlled by evaporating electrode material in a narrow gap may behave differently. These very short arc columns will not be "blown" away by the magnetic field because maintaining the arc column within a conductive pocket of copper vapor is energetically advantageous. The standing long-living high-current arc, when formed, should be a major erosion factor.

"ArcLess" Open Gaps

While arcing is the predominant mechanism for opening a gap, some initial part of this process is achieved with a diffuse current. Since approximately 1 J/cm is required to remove 0.2 mm of a conductive slag sub-layer from a gap, the entire gap would be cleaned by a diffuse current in about 100 msec. The cleaning process is accelerated after the arc is formed due to the instability/contraction of the slag current. Even after the arc is extinguished by magnetic field "blowing" and/or by the voltage drop associated with a potassium deposit, the gap may maintain its relatively high voltage and again conduct high current in the diffuse mode for some time. The characteristic time for a gap to open is usually about 1 minute, while the time required to form a potassium deposit sufficient to extinguish the arc is only a few seconds. Thus an interplay between the potassium deposit and diffuse current arcing processes takes place in an open gap. Direct observations of arcing and time-resolved voltage measurements are needed to proportionate arc current versus diffuse current transfer modes.

*This work was sponsored by the U.S. Department of Energy under Contract No. DE-AC22-87PC90274, Subcontract No. CX5136D58S and Contract No. DE-AC22-84PC70507.

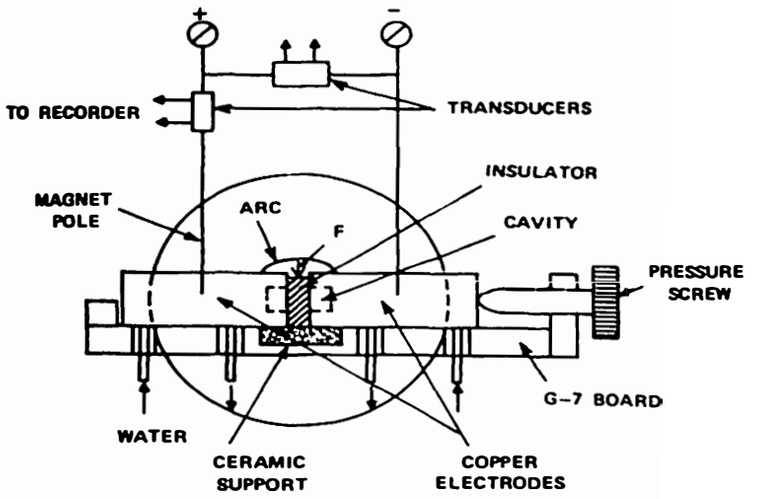

Fig. 1 Sketch of the Interelectrode Arcing Test Rig

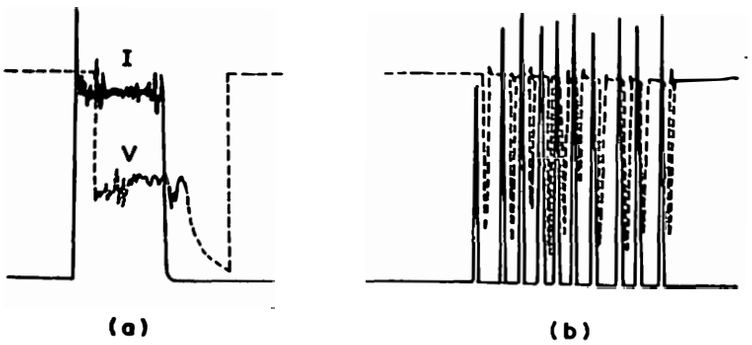

Fig. 2 Current and Voltage Records of Interelectrode Arcing, V_o ~ 250 V, B ≈ 1.35; 1.7 mm, BN Insulator
a) Electrodes without Cavity
b) Electrodes with Cavity, Alternate Arc Ignition

TABLE 1 CHARACTERISTICS OF ARCING BREAKDOWN OF INTERELECTRODE INSULATORS IN A MAGNETIC FIELD

INSULATOR THICKNESS (GAP) mm	MAGNETIC FIELD STRENGTH T	CURRENT A	POWER kW	ENERGY kJ	POWER/ GAP W/mm	ENERGY MASS LOSS J/mg
0.95 BN	1.3	21	1,7	6	1800	165
1.75	1.3	23	1,85	11	1050	122
1.75	1.3	35	2,8	15	1600	162
1.70	1.45	23	1,9	10	1100	115
1.70	0.8	23	1,7	9	1000	90
4.1	1.3	36	4,2	19	1020	100
4.8	1.3	36	4,3	32	900	94
4.0 Si_3N_4	1.3	23	2,4	10	600	52
6.5	1.3	36	4,8	18	740	55
10.8	1.3	36	4,0	22	370	46

TABLE 2 EROSION OF METAL ELECTRODES BY ARC DISCHARGE IN MAGNETIC FIELD

Experimental Conditions	Erosion Rate, μg/Coulomb Anode		Cathode	
B parallel to gap length 0.02 < B < 0.1T I = 20A	Cu	2	Cu	~ 0.5
B perpendicular to gap length 0.01 < B < 0.02T I = 20-30A	Cu W/Cu	0.8 0.5	Cu	~ 0.3
B = 0 I = 25A	Cu	5	Cu	2

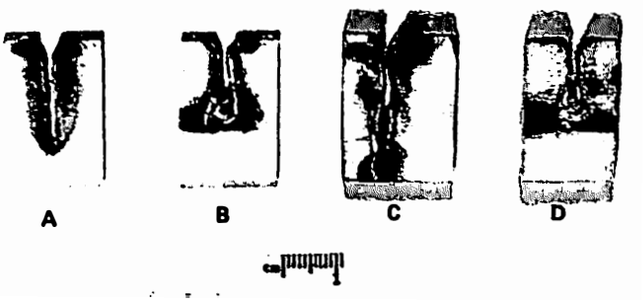

Fig. 3 Arcing Cuts of the Interelectrode BN Insulator (Photo 5431-1)

a) 1.7 mm Thickness, without Cavity
b) 1.7 mm Thickness, with Cavity
c) 4.1 mm Thickness, without Cavity
d) 4.1 mm Thickness, with Cavity

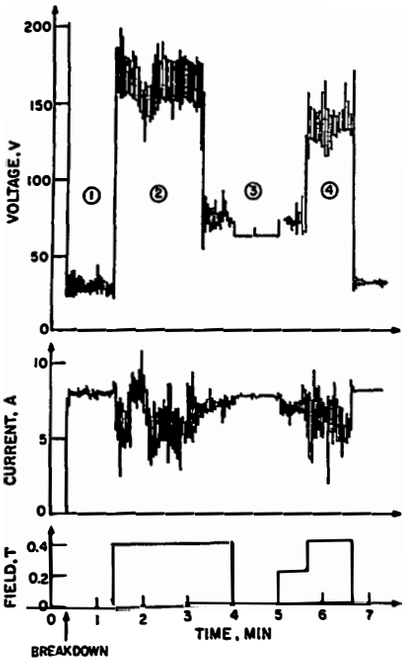

Fig. 4 Arcing Modes in the Presence of Slag
1 Arc Burns Inside the Slag Cavity
2 Open Arc "Detached" by Magnetic Field
3 Current Through a Slag "Bridge"
4 Arc "Detached" by Magnetic Field

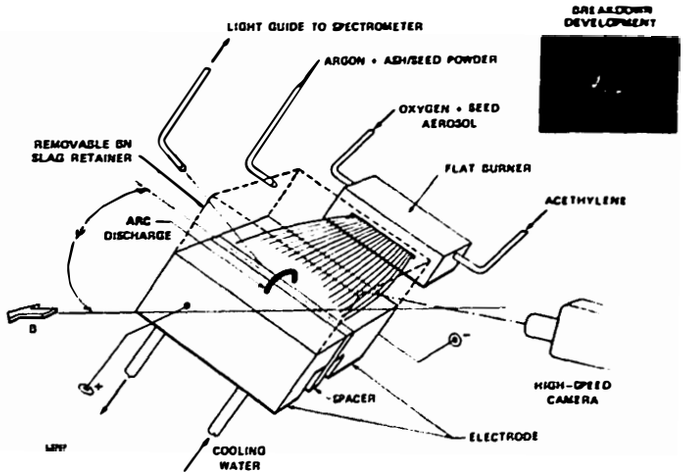

Fig. 5 Sketch of the Interelectrode Arcing Test Set-up II, Unslagged Conditions

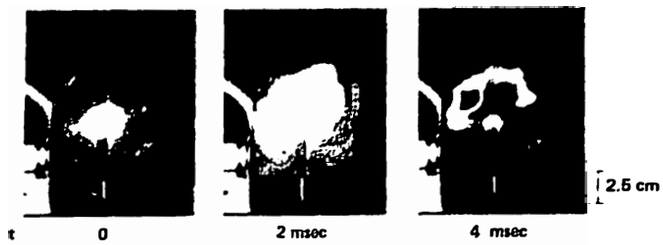

Fig. 6 Typical Sequence of Events for Interelectrode Arcing in a Magnetic field Parallel to the Gap. I = 20A, B = 0.05T, 500 frames/sec, 10^{-4} sec exposure

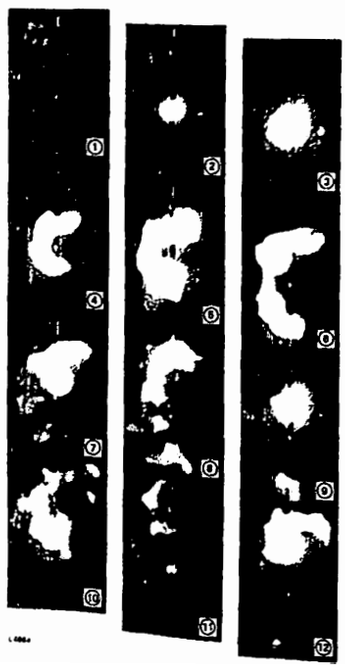

Fig. 7 Sequence of Events for Interelectrode Arcing in a Magnetic Field Perpendicular to the Electrode Surface. I = 30A, BN = 0.02T, 500 frames/sec, 10^{-4} sec exposure

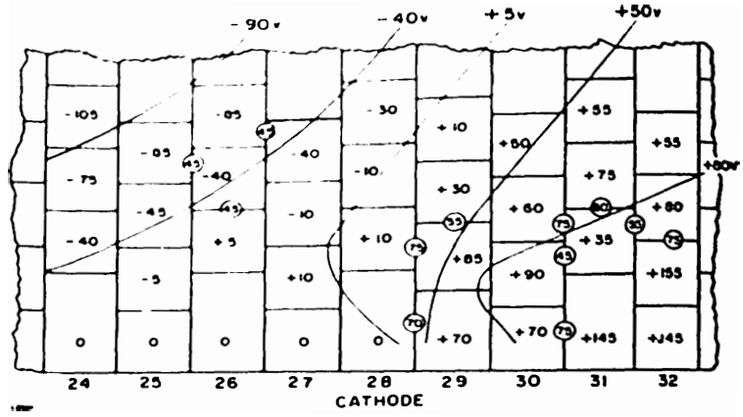

Fig. 8 Typical Voltage Distribution Map Over the Mk VII Sidewall (Near Cathode)

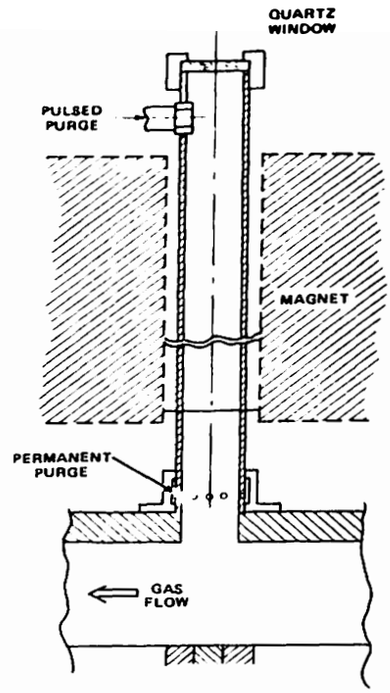

Fig. 9 Design of the Sidewall Optical Port

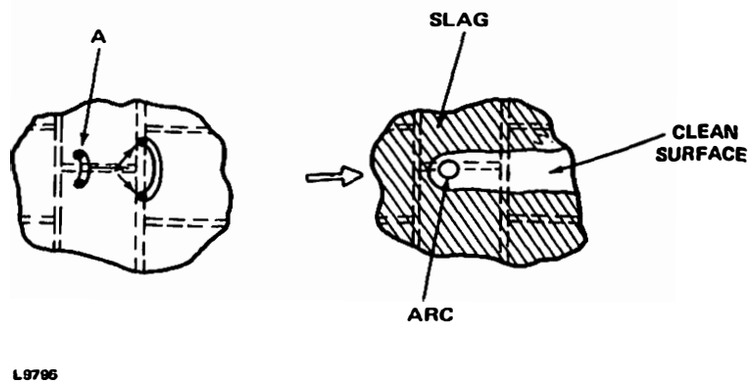

A) B)

Fig. 10 Patterns of Sidewall Arc Movement (a) and Slag Melting (b)

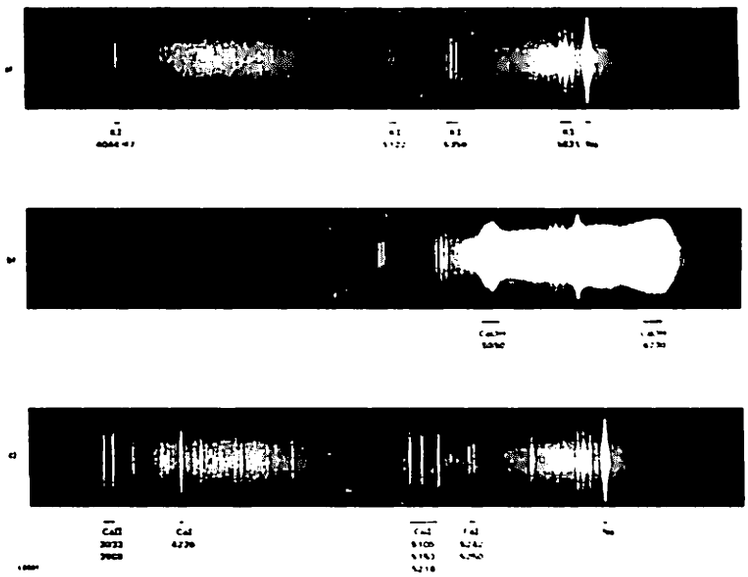

Fig. 11 Spectra of Plasma in Mk VII Extension Section
a) Without Ash Injection
b) With Ash Injection and Slag Layer Formed
c) With Sidewall Arcing

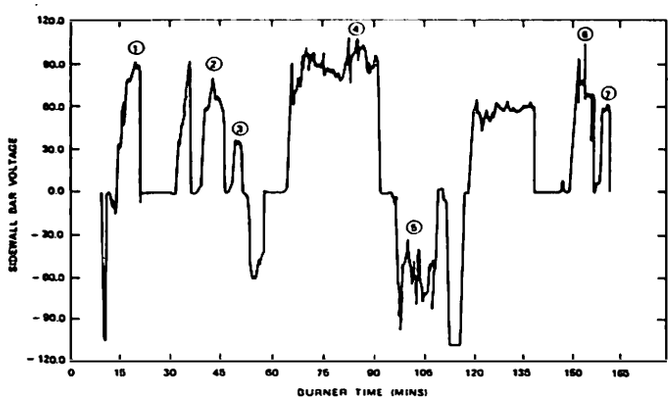

Fig. 12 Real Time Plot of the Interbar (31M-32B) Voltage. 1,2,4,6 - arcing; 3,4 - no arcing 5 - strong arcing

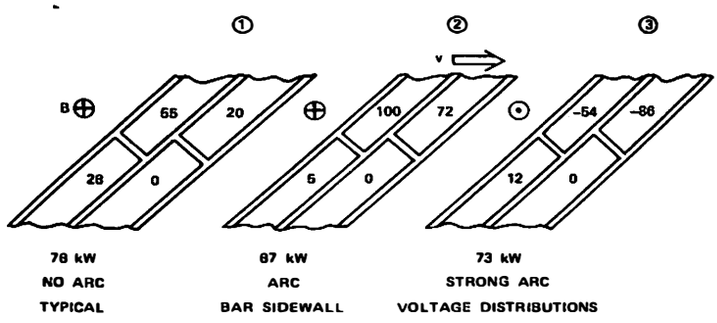

Fig. 13 Voltage Distribution Pattern Corresponding to Selected Burner Times from Fig. 17

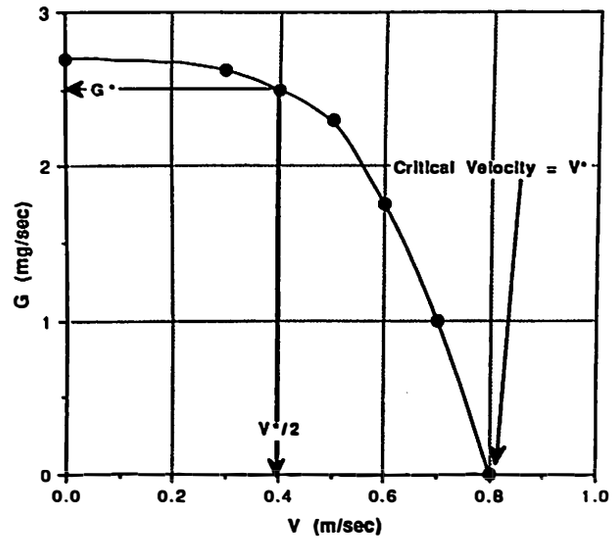

Fig. 14 ARC Erosion vs. Arc Velocity
Rarc = 0.2 mm, Qarc = 500 W, Cu Electrode

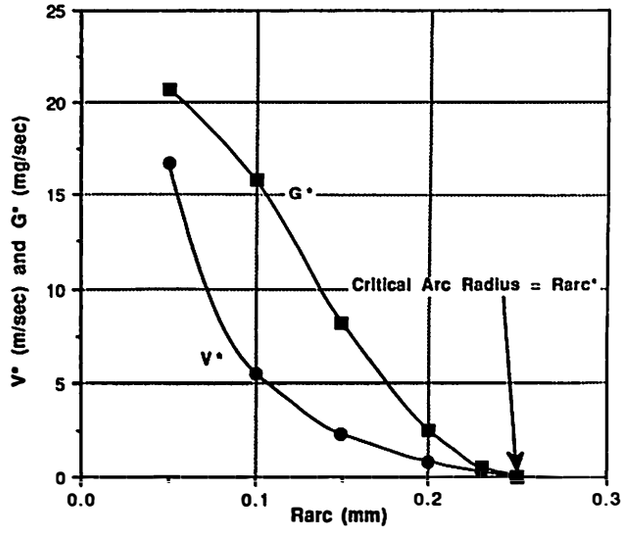

Fig. 15 Arc Critical Velocity and Characteristic Erosion vs. Radius (Qarc = 500 W, Cu electrode)

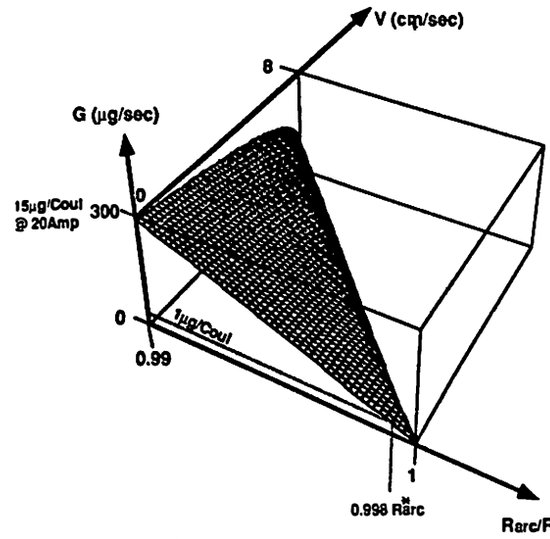

Fig. 16 Arc Erosion vs. Radius and Velocity
Qarc = 500 W, Cu Electrode, Rarc* = 0.25 mm

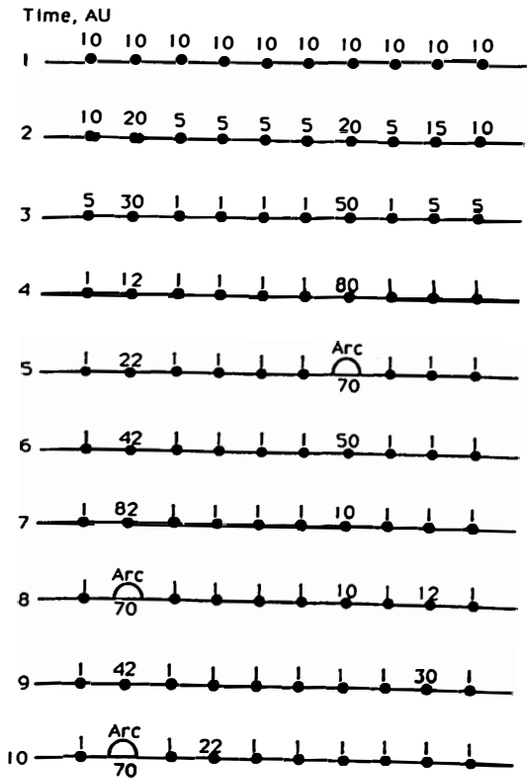

Fig. 17 Example of Hypothetical Voltage Redistribution Sequence Over 10 gap Cathode Wall Segment

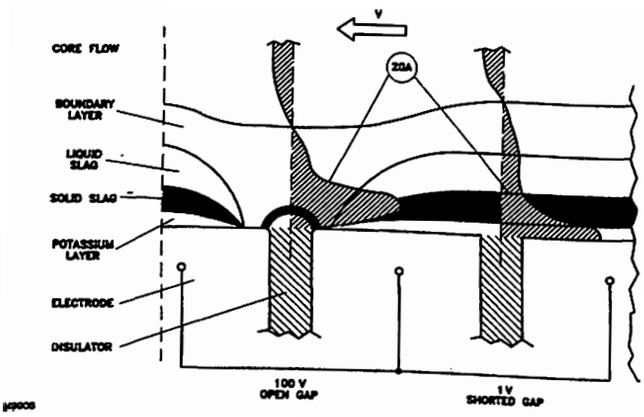

Fig. 18 Hypothetical Current Density Distributions Intercathode Gaps

References

1. Pian, C.C.P., Petty, S.W., and McClaine, A.W., "Experimental Investigation of Factors Affecting the Cathode Wall Slag Layer Resegmentation Frequency," Proceedings of the 26th Symposium on the Engineering Aspects of MHD, Nashville, TN, June 20-22, 1988.

2. Pian, C.C.P., Sadovnik, I., Petty, S.W., and McClaine, A.W., "Voltage-Current Charcteristics of the Insulator Gaps in a Slagging MHD Generator," Proceedings of the 26th Symposium on the Engineering Aspects of MHD, Nashville, TN, June 20-22, 1988.

3. Cott, D.W., "Slag Behavior in MHD Generators: Physical Phenomena and Engineering Consequences," Proceedings of the 26th Symposium on the Engineering Aspects of MHD, Nashville, TN, June 20-22, 1988.

4. Avco Research Laboratory, Inc., "MHD Channel Development," Quarterly Progress Report, Contract No. DE-AC22-84PC70607, July 1986.

5. Podmoshenky, I.V., et al., "High Temperatures, 6, 1130, 1968.

6. Unkel, W. and Blackman, L., Journal of Energy, 7, 272, 1983.

7. Hruby, V.J. and Weiss, P., "Experimental Investigations of the Fault Power in a Segmented MHD Generator," 19th Symposium on Engineering Aspects of MHD, Tullahoma, June 1981.

8. Bashilov, V.A., Makarov, Y.V. and Sorokin, V.Y., "Study of Arc-Quenchers for MHD Generator Anode Wall," 19th Symposium on Engineering Aspects of MHD, Tullahoma, June 1981.

9. Guile, A.E. and Hitchcock, J. Phys. D: Appl. Phys., Vol. 7, 597, (1974).

10. K. Nobata and M. Kurokawa, Japanese Journal of Applied Physics, Vol. 28, 501, 1989.

11. N. Rykalin, A. Uglov, A. Kokora, "Laser Machining and Welding", Mir Publishers, 1978.

12. I.I. Beilis, "Thermal Conditions for the Metal Framework of a Combined MHDG Electrode in a Contracted Discharge", High Temperature Physics, Vol. 24, 1173, 1986.